Saravanan Elanchezhian ✉
Anitha G

https://doi.org/10.21278/TOF.471033221
ISSN 1333-1124
eISSN 1849-1391

SOFTWARE IN-LOOP SIMULATION OF A QUAD TILT ROTOR UNMANNED AERIAL VEHICLE FOR TRANSITION CONTROL

Summary

This paper presents a hybrid unmanned aerial vehicle configuration, the quad tilt rotor (QTR), which combines both the tandem wing configuration and the quadrotor configuration using a tilt mechanism. The paper focuses on the vehicle configuration, transition control scheme and modified proportional-integral-derivative (PID) control. The effectiveness of a tilt rotor configuration depends on its smooth transition from rotary wing to tandem wing flight during take-off and vice-versa during landing. An autonomous transition control scheme for the QTR using a modified PID controller is proposed to maintain desirable attitudes during transition. The derivative control of error term in a conventional PID controller is replaced by the rate of change of the control parameter in the modified PID controller. The modified PID controller provides the desired response with significantly reduced oscillations and actuator control effort than the conventional PID controller. The QTR configuration is simulated in a software-in-the-loop (SIL) simulation using MATLAB Simulink and the X-Plane simulator to analyze the controller performance and flight characteristics during transitions from rotary wing to tandem wing flight during take-off and vice-versa during landing. The simulation is performed with and without atmospheric disturbance and the simulation results showed acceptable deviation in attitude during the transition even under atmospheric disturbances.

Key words: *transition control, dynamic modelling, software-in-the-loop simulation, quad tilt rotor, X-Plane.*

1. Introduction

Advances in sensor technology [1–3], electronics, guidance, and controls, and in multirotors in particular, have fostered the development of unmanned aerial vehicles (UAVs) over a decade. Fixed-wing aircraft cannot hover, and the growing demand for aerial imaging and surveillance drove the market interest toward multirotors which are capable of hovering. Unlike fixed-wing aircraft, rotary-wing aircraft like multirotors are capable of vertical take-off and landing (VTOL), avoiding the runway requirement. In addition, if the same power is considered, multirotors are less energy efficient and have less endurance than fixed-wing aircraft. The above considerations led to the development of tilt rotors that have advantages of both fixed wings and multirotors.

Research on convertible aircraft capable of vertical take-off and landing with convertible horizontal flight has been carried out extensively [1, 4, 5] to overcome the disadvantages of

fixed-wing and multirotor vehicles. Different types of tilt configurations have been attempted over the years, such as tilt wing [5, 6], partial tilt wing [7], collective thrust transitioning (CTT) [5, 8, 9], tilt-rotor [5, 10–12], etc. Saeed et al. [5] summarised the merits and demerits of hybrid convertible configurations. Tilt wing aircraft require heavy and powerful actuators to tilt the entire wing but have good aerodynamic performance during transition. Tilt wing and flying wing configurations are vulnerable to crosswind, and hence it is not easy to land on moving decks. Tilt rotors are not very vulnerable to crosswinds and require smaller actuators but have poorer aerodynamic performance during transition than tilt-wing configurations. Partial tilt-wing aircraft are intermediate between tilt-rotor and tilt-wing aircraft. Partial tilt-wing aircraft are also vulnerable to crosswinds but slightly less than tilt-wing aircraft. The advantage and the need for convertible type aircraft over fixed-wing aircraft are their ability to hover, take off, and land vertically. Tilt wing, partial tilt-wing, and CTT configurations are vulnerable to crosswind during hover, take-off, and landing.

Nomenclature

b	wing span
$\bar{C}$	mean aerodynamic chord
g	acceleration due to gravity
h	altitude
L_W	lift due to crosswind at hover condition
m	mass of the aircraft
q_0	dynamic pressure
P, Q, R	angular velocities about x-, y- and z- axes in body frame
R	range between current location and desired waypoint
R_{TH}	threshold range
R_e	radius of Earth (6,371 km)
S	wing planform area
T_H	hover thrust
U, V, W	linear velocities along x-, y- and z- axes in body frame
V_W	disturbance wind velocity
V_{X_B}	velocity component along x-axis in body frame (calculated from X-Plane data)
α	angle of attack
β	sideslip angle
$\delta_a, \delta_e, \delta_r$	aileron, elevator and rudder deflection angle
ϕ, θ, ψ	Euler angles (roll, pitch and heading)
φ	latitude
λ	longitude
ξ	tilt angle
τ	torque
ψ_W	disturbance wind direction in the Earth axis system

In general, quad tilt rotors can be flown as fixed-wing aircraft or as short take-off and landing (STOL) aircraft with partial tilt when there is a failure of one or more transition actuators. The above reason made the quad tilt rotor the vehicle configuration of choice in this paper. A tandem wing type quad tilt-rotor, as shown in Fig. 1, is considered in this paper. The tandem wing configuration is selected as it allows for various structural modifications in the future, such as variable wing sweep and variable dihedral angle. Thomas Lambert et al. [13] reported that dihedral angles of the two wings have a significant impact on the lift; some configurations lead to an increase in the lift coefficient of up to 25%.

X-Plane flight simulator is used in this paper to simulate the nonlinear vehicle dynamics to overcome the difficulties in the conventional design approach. The conventional design approach requires a suitable mathematical model of the vehicle, which requires computational fluid dynamics (CFD) analysis or wind tunnel tests to obtain force and moment coefficients for

different flight conditions. Further, the accuracy of the mathematical model depends on the accuracy of the CFD or wind tunnel data and different parameters considered during modelling. Also, it is difficult to model the transition dynamics as the CFD/wind tunnel data are generally collected for a different set of static conditions, and the transition behaviour changes for a different rate of transition. X-Plane is one of the advanced flight simulators approved by the Federal Aviation Administration (FAA) as a training simulator because of its high-fidelity simulation of flight models and visualization. Based on a survey report by Jeff Craighead et al. [14] on commercial and open-source flight simulators, X-Plane is one of the best flight simulators. X-Plane is also used for system identification of UAVs [15–17], as a test platform [18–20] for controller performance and for testing new aircraft designs including a tiltrotor aircraft [21]. X-Plane calculates the aircraft response using the Blade element theory based on a current scenario. The aircraft response is close to actual flight due to the use of the blade element theory, which makes X-Plane the preferred choice. The mathematical model of the QTR UAV presented in Section 2 of this paper is used as a framework to understand the control requirements of the proposed vehicle configuration.

The different types of existing tilt rotors and their different control schemes were summarised by Liu Zhong et al. [4], and PID controllers were also used for attitude and position control in the helicopter mode. Conventional PID controllers were also used in missile seekers [22]. A survey of hybrid UAVs by Adnan Saeed et al.[5] compared different control laws used in hybrid UAVs. Except for PID controllers, most linear and nonlinear controllers require a proper mathematical model, full state feedback, or precise knowledge of the aerodynamic coefficients [5]. Since X-Plane is used to simulate an aircraft dynamic model, it is not easy to design a controller that requires a mathematical model or precise knowledge of the aerodynamic coefficients. The disadvantage of the PID controller is that it is not optimal and has poor robustness compared with the robust controller when the system encounters multiple challenges [5]. The PID controller also requires less memory and low computational power than other robust controllers. Because of these reasons and the simulation scenario, a modified PID controller is used in this paper which does not require the knowledge of the UAV mathematical model.

2. Modelling of a quad tilt rotor UAV

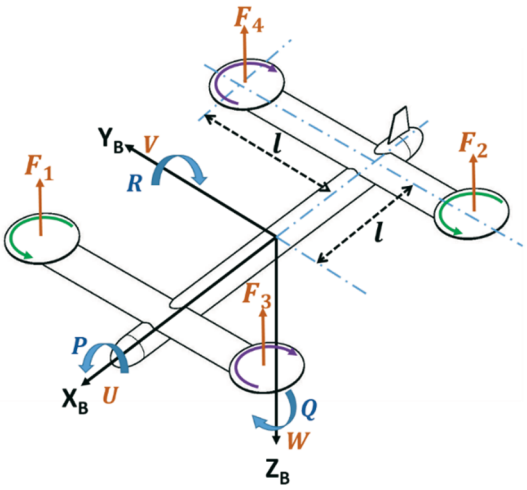

Fig. 1 Aircraft equations of motion

The body axis coordinate system (Z_B, Y_B, Z_B) and the free body diagram of the quad tilt engine aircraft are shown in Fig. 1. The aircraft consists of four rotors arranged in the tandem wing configuration as presented in Fig. 1.

A QTR UAV is a vertical take-off horizontal transition type hybrid vehicle with four rotors. In this configuration, all the four rotors are tilted simultaneously by an angle ξ about the aircraft lateral axis, as shown in Fig. 2. Take-off and landing can be performed vertically ($\xi = 90^{o}$) and during cruise flight, the tilt angle is maintained as zero.

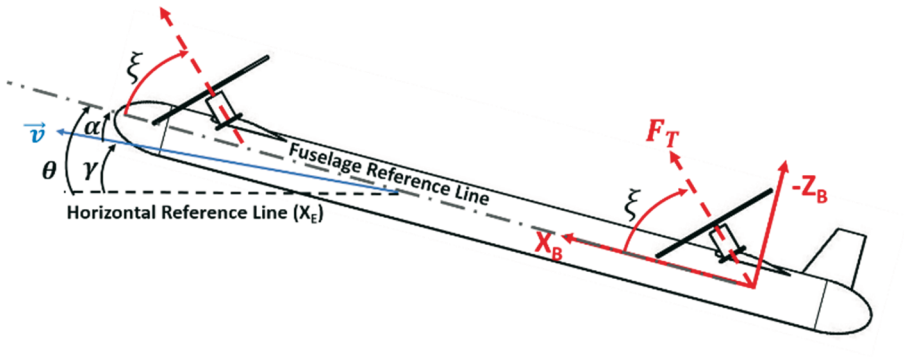

Fig. 2 Side view of QTR UAV showing the tilt angle

Equations of motion (EOM) describing the vehicle dynamics [23, 24] are essential in understanding the behaviour of the aircraft. The EOM can be derived by equating the applied forces and moments to the aircraft response. The force and moment equation defined in the rotating reference frame (body axis) is defined as

$$\left[\vec{F}\right]_B = m\left\{\left[\vec{\dot{v}}\right]_B + (\vec{\omega} \times [\vec{v}]_B)\right\} \tag{1}$$

$$\tau = I_{cm}\vec{\Omega} + \{\vec{\omega} \times (I_{cm}\vec{\omega})\} \tag{2}$$

where,

$$[\vec{v}]_B = U\hat{\imath} + V\hat{\jmath} + W\hat{k}$$

$$\vec{\omega} = P\hat{\imath} + Q\hat{\jmath} + R\hat{k}$$

$$\vec{\Omega} = \vec{\dot{\omega}} = \dot{P}\hat{\imath} + \dot{Q}\hat{\jmath} + \dot{R}\hat{k}$$

$[\hat{\imath}, \hat{\jmath}, \hat{k}]$ represents the unit vectors acting along the defined axis system. $\vec{v}$, $\vec{\omega}$ and $\vec{\Omega}$ are the vectors representing linear velocity, angular velocity, and angular acceleration, respectively. I_{cm} is the 3×3 inertia matrix defined about the aircraft centre of mass.

2.1 Forces and moments

The forces acting on the vehicle are as follows:

$$\begin{bmatrix} F_x \\ F_y \\ F_z \end{bmatrix}_B = \begin{bmatrix} F_{G_x} + F_{A_x} + F_{T_x} \\ F_{G_y} + F_{A_y} + F_{T_y} \\ F_{G_z} + F_{A_z} + F_{T_z} \end{bmatrix}_B$$

F_{G_x}, F_{A_x} and F_{T_x} are the gravitational, aerodynamic and thrust force components represented along the body x-axis, respectively, and similarly for the y- and z-axes.

The gravitational, aerodynamic and thrust force can be conveniently represented in the Earth, stability and body axis systems. The gravitational and aerodynamic forces acting on the aircraft are represented in the body frame using a rotation matrix [23] to resolve the net resultant force vector.

$$\left[\vec{F_G}\right]_B = R_E^B\left[\vec{F_G}\right]_E = R_E^B\begin{bmatrix}0\\0\\mg\end{bmatrix}_E \tag{3}$$

$$\left[\vec{F_A}\right]_B = R_S^B\left[\vec{F_A}\right]_S = R_S^B\begin{bmatrix}-D\\F_{A_y}\\-L\end{bmatrix}_S \tag{4}$$

$$\left[\vec{F_T}\right]_B = \begin{bmatrix}\Sigma F_i\cos\xi\\0\\-\Sigma F_i\sin\xi\end{bmatrix}_B \tag{5}$$

Equations (3-5) represent different forces acting on the aircraft and ΣF_i is the sum of forces generated due to motors 1 to 4.

$\left[\vec{F_G}\right]_E$ and $\left[\vec{F_A}\right]_S$ are the gravitational and aerodynamic force vectors represented in the Earth axis and stability axis system. The north-east-down (NED) frame is the Earth axis system used to represent the gravitational force. The 3×3 rotation matrix R_E^B is used to represent the gravitational force defined in the Earth axis system in terms of the vehicle body axis system and vice versa by R_B^E. It represents three sequential rotations about z-, y- and x-axes and the matrix representing this sequence of rotation is as follows:

$$R_E^B = \begin{bmatrix}C\theta C\psi & C\theta S\psi & -S\theta\\ S\phi S\theta C\psi - C\phi S\psi & C\phi C\psi + S\phi S\theta S\psi & S\phi C\theta\\ S\phi S\psi + C\phi S\theta C\psi & C\phi S\theta S\psi - S\phi C\psi & C\phi C\theta\end{bmatrix} \tag{6}$$

$$R_B^E = (R_E^B)^T$$

$C\theta, S\theta$ denotes $\cos\theta$ and $\sin\theta$, respectively. Similarly, the stability axis to the body axis rotation matrix is defined as

$$R_S^B = \begin{bmatrix}C\alpha & 0 & -S\alpha\\ 0 & 1 & 0\\ S\alpha & 0 & C\alpha\end{bmatrix} \tag{7}$$

$$\propto = \tan^{-1}\frac{W}{U} \tag{8}$$

The stability axis system coincides with the aircraft body axis system, but it is rotated about the aircraft lateral axis (Y_B) by an angle of attack, α. Linear acceleration in the body can be calculated using equations (3-8), as shown in equation (9) which can be integrated to obtain linear velocity and position. Linear acceleration, velocity and displacement in terms of the Earth axis system can be obtained using the rotation matrix $R_B^E = (R_E^B)^T$.

$$\left[\vec{\dot{v}}\right]_B = \left(\frac{\left[\vec{F_G}\right]_B + \left[\vec{F_A}\right]_B + \left[\vec{F_T}\right]_B}{m}\right) - (\vec{\omega} \times [\vec{v}]_B) \tag{9}$$

The moments acting in the vehicle are

$$\tau = \begin{bmatrix}l(-F_1 + F_2 + F_3 - F_4)\sin\xi + \bar{L}\\ l(F_1 - F_2 + F_3 - F_4)\sin\xi + M\\ (\mathcal{M}_1 + \mathcal{M}_2 - \mathcal{M}_3 - \mathcal{M}_4)\sin\xi + N\end{bmatrix}, \tag{10}$$

where $F_{1,2,3,4}$ are the forces generated by the individual motors; l is the distance between the motor and the vehicle centre of mass along the x- and y-axes; $\mathcal{M}_{1,2,3,4}$ are the moments produced

by each motor perpendicular to the plane of rotation of the propeller; $\bar{L}, M, N$ are the aerodynamic moments about the x-, y- and z-axes, respectively. The factors affecting the moments are given in equation (11).

$$\bar{L} = q_0 S b C_{\bar{L}}(\beta, P, R, \delta_a) \tag{11a}$$

$$M = q_0 S \bar{c} C_M(\alpha, Q, \delta_e) \tag{11b}$$

$$N = q_0 S b C_N(\beta, P, R, \delta_a, \delta_r) \tag{11c}$$

$$q_0 = \frac{1}{2}\rho v^2$$

$$\beta = \sin^{-1}\frac{V}{v}$$

$$v = \sqrt{U^2 + V^2 + W^2}\,,$$

where v is the magnitude of the velocity vector; $C_{\bar{L}}(\beta, P, R, \delta_a)$ is the rolling moment coefficient about the x-axis as a function of β, P, R, δ_a and similarly for C_M and C_N for the pitching and the yawing moment coefficient, respectively. Angular acceleration in the body frame can be calculated as shown in equation (12) which can be integrated to obtain the angular velocity.

$$\overrightarrow{\Omega} = \frac{\tau - \{\vec{\omega} \times (I_{cm}\vec{\omega})\}}{I_{cm}} \tag{12}$$

The components of the angular velocity of the vehicle in the body frame (P, Q, R) is related to the derivatives of Euler angles, as shown in equation (13). Therefore, the Euler rate calculated from equation (13) can be integrated to obtain Euler angles.

$$\begin{bmatrix} P \\ Q \\ R \end{bmatrix} = \begin{bmatrix} 1 & 0 & -\sin\theta \\ 0 & \cos\phi & \sin\phi\cos\theta \\ 0 & -\sin\phi & \cos\phi\cos\theta \end{bmatrix} \begin{bmatrix} \dot{\phi} \\ \dot{\theta} \\ \dot{\psi} \end{bmatrix} \tag{13}$$

2.2 Control of the quad tilt rotor

Differential thrust is used to control the attitude and motion of the vehicle in the quadcopter mode [25], and primary control surfaces (aileron, elevator and rudder) are used for attitude and motion control when the engine tilt angle is zero. During the fixed-wing configuration and transition phase, the speed of all motors is maintained the same. The differential thrust generated by each rotor achieves control of the vehicle in the quadcopter configuration. The speed of an individual motor depends on thrust, pitch, roll and heading requirements. The required speed of the motor is calculated using equation (14):

$$\begin{bmatrix} n_1 \\ n_2 \\ n_3 \\ n_4 \end{bmatrix} = \begin{bmatrix} 1 & -1 & 1 & -1 \\ 1 & 1 & -1 & -1 \\ 1 & 1 & 1 & 1 \\ 1 & -1 & -1 & 1 \end{bmatrix} \begin{bmatrix} \Delta n_T \\ \Delta n_\phi \\ \Delta n_\theta \\ \Delta n_\psi \end{bmatrix} \tag{14}$$

n_{1-4} – speed of motors 1 to 4

Δn_θ – change in speed required to achieve a desired pitch angle (depends on error valve, θ_{err}) and similarly for thrust (altitude), roll and heading.

The direction of rotation of the motors is configured as shown in Fig. 1 so that when all motors run at constant speed, moments produced by motors 1 and 2 exactly balance the moments produced by other two motors. This arrangement provides yaw control during vertical flight and zeroes roll moment during horizontal flight, similarly to a twin-engine aircraft. The engine tilt angle ξ is controlled based on the transition command and thrust vector control.

3. X-Plane simulator

X-Plane is a commercially available flight simulator developed by Laminar Research. X-Plane provides additional software to design custom aircraft and airfoils using Plane Maker and Foil Maker. X-Plane calculates the aircraft response using the blade element theory based on a current scenario. X-Plane version-10 Global edition is used to test and analyse the aircraft response during the transition phase. X-Plane also provides a feature that can simulate a flight under actual weather conditions. In this paper, raw METAR (Meteorological Terminal Aviation Routine Weather Report) data is downloaded to simulate actual weather conditions.

3.1 Plane Maker

Plane Maker is software provided along with X-Plane-10 to design and configure custom aircraft [26, 27]. The aircraft specifications, such as fuselage dimensions, wingspan, chord, control surface dimensions and their deflection limits, propeller dimensions, engine type, etc., are used to design the aircraft. Electric motors are used as engines for this QTR UAV. The moment of inertia is calculated using XFLR5 by providing mass distribution data, and the center of gravity is fixed at the midpoint between the front and the rear wings. The mass radius of gyration calculated from the mass moment of inertia is used in Plane Maker during the design process. The quad tilt rotor configuration designed by using Plane Maker for X-Plane 10 is loaded in the X-Plane simulator during simulation. Fig. 3 shows a QTR aircraft designed in the X-Plane simulator.

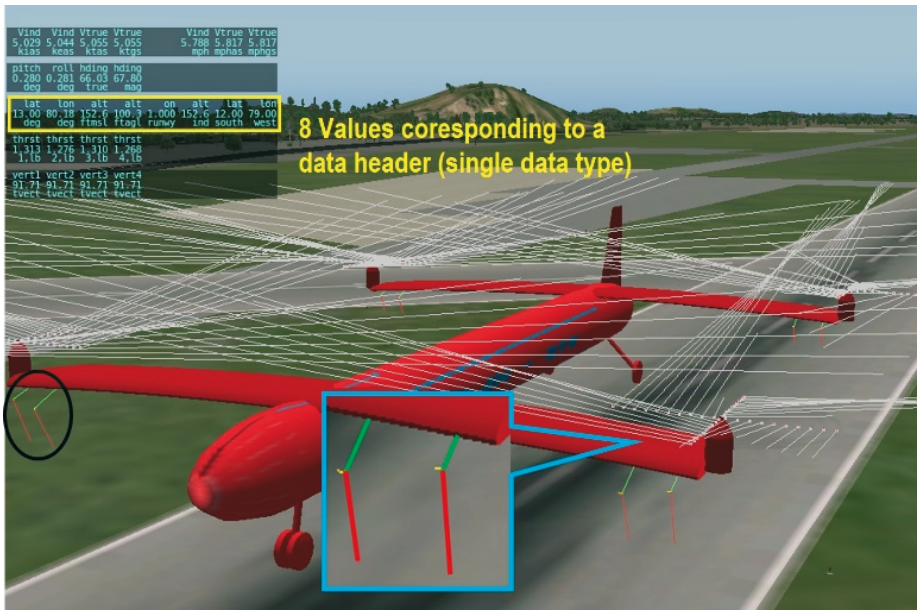

Fig. 3 Designed aircraft in X-Plane simulation environment

Table 1 Aircraft specification

Parameter	Value	Parameter		Value
Wingspan	100 cm	Aileron & Elevator	Dimension	20 x 4.5 cm
Chord	15 cm		Deflection	±15 deg
Vertical tail area	150 cm^2	Rudder	Dimension	9.5 x 4 cm
All up mass	3.4 kg (7.5 lb)		Deflection	±35 deg
Engine power	0.45 hp	Tilt angle		0 – 110 deg
Propeller diameter, pitch	10 inch, 4.5	Tilt rate		30 deg/sec
Mass moment of inertia	I_{xx} = 0.36395; I_{yy} = 0.71960; I_{zz} = 1.07755 kg · m^2			

The physical dimensions and specifications that are used to design the aircraft in Plane Maker are provided in Table 1. The aileron and elevator dimensions specified in Table 1 are for a half wing.

3.2 UDP Communication

X-Plane uses UDP communication for the exchange of data. UDP communication is set up between X-Plane and MATLAB by specifying the IP address and the port to which the data is to be sent and received. The type of data to be sent or received (Ex: airspeed, altitude, latitude, longitude, etc.) is selected from the available 133 data set in X-Plane.

X-Plane sends and receives data in a specific format, as shown in Fig. 4. The fifth byte of the packet header is a “don't care” byte when the data is received from X-Plane, and it must be "0" (zero) when the data is transmitted to X-Plane.

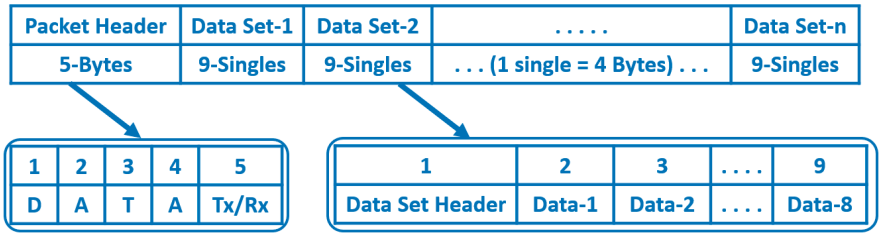

Fig. 4 UDP data format

The data from and to X-Plane are received and transmitted in Simulink using the UDP receive and send block, respectively. The data sent and received in Simulink are formatted and decoded according to the UDP data format shown in Fig. 4.

4. Research methodology

Autonomous flight simulation is performed using waypoint navigation [28, 29]. Only two waypoints, take-off and landing coordinates, are used in the simulation to demonstrate the transition flight. Transition is performed based on altitude and the range for take-off and landing, respectively. The aircraft is in the quadcopter mode when the tilt angle is 90° and in the tandem mode when the tilt angle is zero. Thrust vector control is also performed by varying the tilt angle to maintain the desired forward velocity in the aircraft body frame (V_{X_B}).

The heading angles and range are calculated using the Haversine formula shown in equations (15-16) based on the current and desired coordinates.

$$a = \sin^2\left(\frac{\varphi_2-\varphi_1}{2}\right) + \cos\varphi_1 \cdot \cos\varphi_2 \cdot \sin^2\left(\frac{\lambda_2-\lambda_1}{2}\right)$$

$$R = 2 \cdot R_e \cdot \text{atan2}(\sqrt{a}, \sqrt{1-a}) \tag{15}$$

$$\psi = \text{atan2}((\sin(\Delta\lambda) \cdot \cos\varphi_2)\,,\ (\cos\varphi_1 \sin\varphi_2 - \sin\varphi_1 \cos\varphi_2 \cos(\Delta\lambda)) \qquad (16)$$

$$\Delta\lambda = \lambda_2 - \lambda_1$$

The transition is performed based on altitude during take-off and threshold range during landing. Landing is initiated when the aircraft longitudinal component of velocity goes below the desired value.

5. Quad tilt rotor simulation

Simulation of an autonomous flight is performed to test and analyse the transition and controller performance during the transition phase. The different flight phases involved in the simulation are vertical take-off, horizontal transition, cruise flight, vertical transition, and landing. The mathematical model defined in Section 2 serves to understand the different forces and moments acting on the vehicle and to develop a framework for flight control. The difficulty in performing the simulation entirely based on the mathematical model is in providing the constants (Inertia matrix, $C_{L_\alpha}, C_{D_\alpha}$ etc.) and stability derivatives for simulation. To obtain these values for different flight conditions, an extensive wind tunnel test or a CFD analysis [30, 31] is required. Any existing data for similar fixed-wing aircraft cannot be used effectively as those values are generally restricted to the stall angle. For this quad tilt rotor, the angle of attack may vary from -90^o to 90^o and sometimes slightly above this range if thrust vectoring is used. The correctness of the simulation depends on the accuracy of the constants and stability derivatives. The difficulty in getting these values made X-Plane the simulation environment for this simulation. Roll control in the quadcopter mode becomes yaw control in the tandem mode and has slightly complex dynamics during the transition. During the transition phase, the rotor speeds are held constant to reduce the complexity and to simplify the controller design. Fig. 5 shows the block schematic of the SIL simulation using MATLAB and X-Plane. The figure also provides an overview of the control scheme implemented in MATLAB.

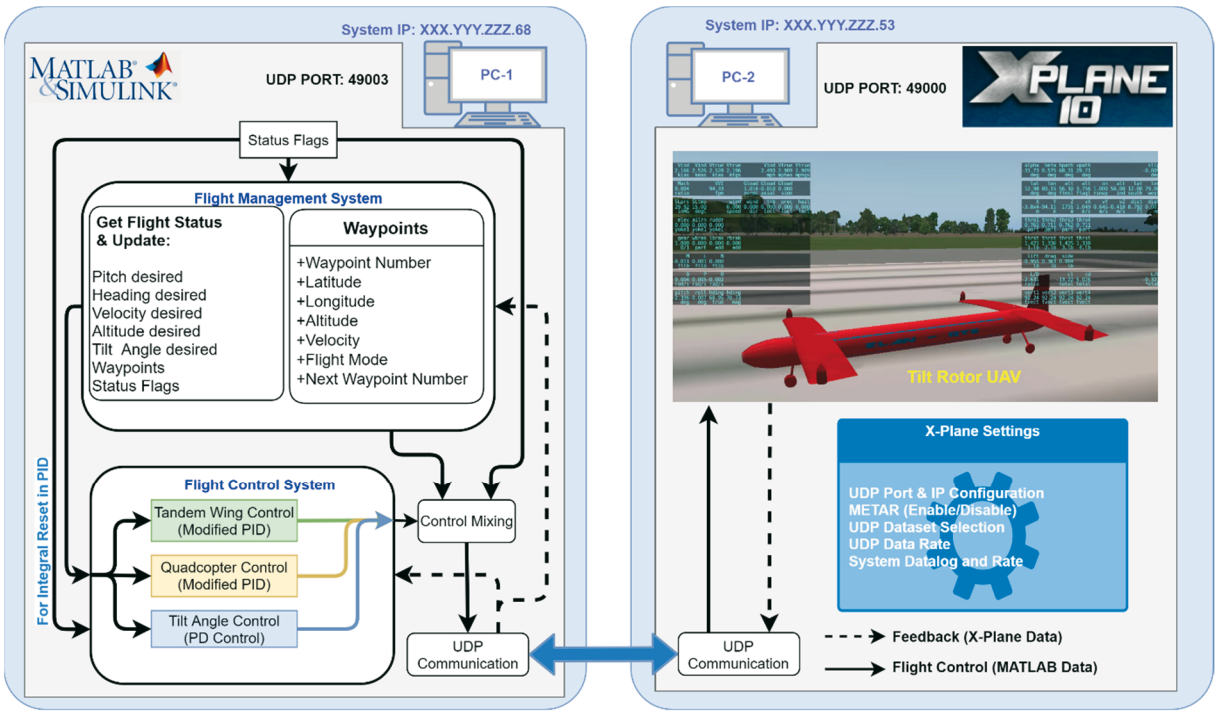

Fig. 5 Software-in-the-loop simulation block schematic using MATLAB and X-Plane

5.1 Modified PID control

Most linear and nonlinear controllers require the mathematical model of the system in state-space form or some other representation to design a controller. It is challenging to design an optimal control scheme without a proper mathematical model. PID controller does not require the knowledge of the UAV model, and hence a modified PID controller is used.

Equations (17-20) show different PID controller implementations for pitch angle control using elevator deflection as a control command. Equation (17) represents the conventional PID controller implementation found in books and papers. Equation (18) represents the MATLAB Simulink implementation of a conventional PID controller where the derivative part is implemented as a combination of the filter with the filter coefficient $\bar{N}$ and derivative part in the s-domain as shown in equation (20). Equation (19) shows the modified PID controller implemented in this paper.

PID controller tuning is performed manually online while the simulation is running by visually looking at the aircraft response and how the individual components of P, I and D are contributing to this behaviour. During the initial PID controller tuning attempts with a conventional PID controller, the derivative term introduced oscillations primarily in the pitch axis as it is inherently unstable for this selected model configuration. By further tuning, to get reduced oscillations, either the response was slow for the optimum control effort, or the control effort was too high for better response. So, the *derivative control of error* term is replaced by the *rate of change of control parameter* (Q in case of the pitch control). Later this concept evolved into the present modified PID controller.

$$\delta_e = K_P\theta_{err} + K_I \int \theta_{err} + K_D \frac{d\theta_{err}}{dt} \tag{17}$$

$$\delta_e = K_P\theta_{err} + K_I \int \theta_{err} + K_D \frac{\bar{N}}{1+\bar{N}\int \theta_{err}} \tag{18}$$

$$\delta_e = K_P\theta_{err} + K_I \int \theta_{err} + K_D(Q_{des} - Q) \tag{19}$$

where, $Q_{des} = \left(\frac{d\theta}{dt}\right)_{des} = \frac{\theta_{err}}{n}$ and $Q = \left(\frac{d\theta}{dt}\right)_{Actual}$

$$\left(\frac{\bar{N}}{s+\bar{N}}\right) s = \frac{\bar{N}}{1+\bar{N}\frac{1}{s}} \tag{20}$$

Equation (19) represents the block schematic shown in Fig. 6. Q_{des} represents the desired rate and Q represents the actual current rate of the aircraft. Here, n is the scaling factor ($n > 1$) based on which the desired rate is fixed as a fraction of the error value (θ_{err}). Higher values of n result in a slow response, and lower values of n provide a fast response but with an increased actuator control effort. The operating range on the actuator control limits the value of n. For this simulation, $n = 3$ provides the desired response. In this method of implementation, the desired rate ($\frac{\theta_{err}}{n}$) changes dynamically based on the current error value. It was observed that this method of a modified PID controller provides a better response with lesser control effort when compared with the conventional PID controller presented in equations (17-18).

In the modified PID controller, the derivate part is replaced by the pitch rate control as shown in Fig. 6. The desired pitch rate is a fraction of error in pitch and the fractional part is adjusted during the tuning process. A smooth, non-aggressive control signal is generated using this modified PID controller. The integral error values are reset during transition based on the transition command (TransFlag) shown in Fig. 8(a).

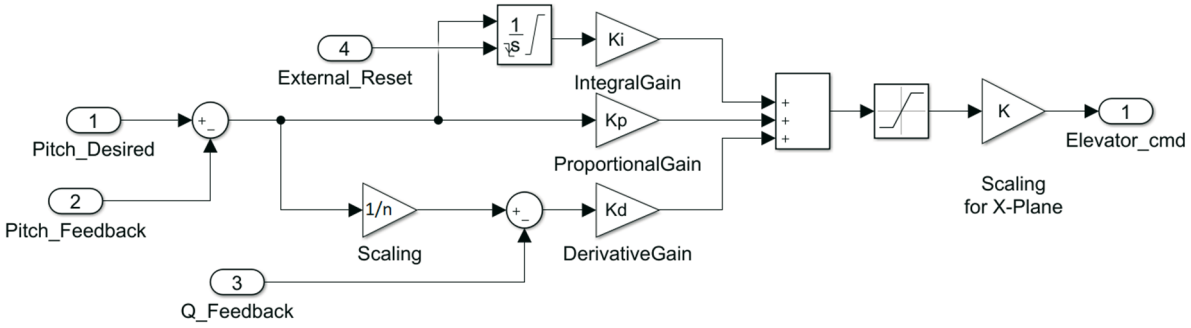

Fig. 6 Block diagram of a modified PID controller

5.2 Thrust vector control

During the vertical flight, it is observed that an aerodynamic force is generated along the longitudinal axis, hence the path traced by the flight is not exactly vertical but slightly inclined. Thrust vector control (TVC) is implemented to cancel the forward aerodynamic force by varying the tilt angle slightly beyond 90º. The TVC operating angle ranges from 88º to 110º. Fig. 7(a) shows different forces acting on the wing during the vertical flight. It also shows the lift and drag force defined for the direction of airflow (freestream velocity). A similar effect is also seen in X-Plane as highlighted in Fig. 3. The green line in Fig. 3 represents the magnitude and direction of the lift force, and the red line represents the magnitude and direction of the drag. The magnitude of this force is high in the slipstream region and negligible in the freestream region. The slipstream region experiences an increased airflow than the free stream area as the slipstream region is directly below the rotor disc. This effect can be seen by comparing Fig. 7(b) to Fig. 3.

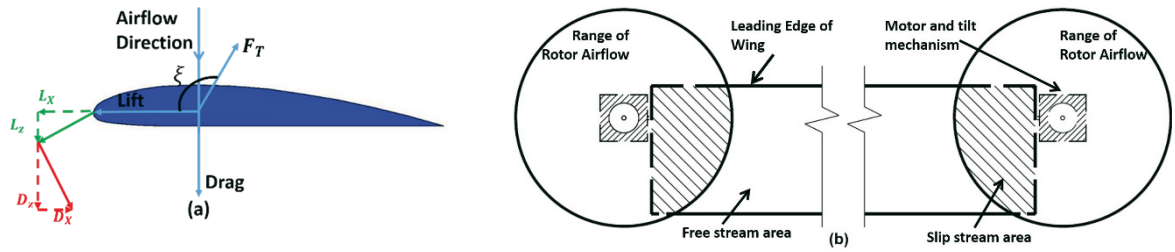

Fig. 7 (a) Aerodynamic force during vertical flight, **(b)** Free stream area and slipstream area of a wing in quadcopter mode

X-Plane provides velocity along the three components of the earth axis system. X-Plane uses the east-up-south coordinate system defined along the x-, y- and z- axes. These velocities are converted to body frame using a rotation matrix as in equation (21).

$$\begin{bmatrix} V_{X_B} \\ V_{Y_B} \end{bmatrix} = \begin{bmatrix} \sin\psi & -\cos\psi \\ \cos\psi & \sin\psi \end{bmatrix} \begin{bmatrix} V_{X_E} \\ V_{Z_E} \end{bmatrix} \tag{21}$$

A modified PD controller is implemented to minimise the velocity along the x-axis in the body frame (V_{X_B}) by controlling the tilt angle. The controller is similar to the modified PID controller without an integral part.

6. Results and discussion

The simulation is performed with and without atmospheric disturbances in X-Plane. The METAR data is used to produce atmospheric disturbance by enabling that option in X-Plane. The controller performance and the aircraft responses are compared for both cases. The control commands, aircraft response and state parameters are logged during the simulation via

MATLAB and X-Plane. The logged data are then used for the performance analysis and comparison.

Fig. 8 shows the aircraft state parameters of interest during the transition phase. During the simulation, the desired altitude was set at 150 ft (45.72 m), and the desired pitch and roll values are set at zero degrees with a true heading of 68.8 degrees. Fig. 8(a) shows the Trans Flag plot for the simulation under disturbed and undisturbed flight conditions. Trans Flag is one of the conditional flags based on which the transition from the quadcopter mode to the tandem mode (if Trans Flag = 1) and vice-versa (if Trans Flag = 0) is performed. This transition (0 to 1) takes place when the altitude goes above the set altitude (150 ft) and the other transition (1 to 0) takes place when the distance to the landing site goes below the threshold value (R_{TH} = 110 m).

Fig. 8(b) shows the tilt angle for both simulation cases. The tilt angle is varied between 0^o and 90^o for transition and from 88^o to 110^o for thrust vector control. The plot shows the tilt angle around the 90^o region over which the thrust vector control takes place.

For the disturbed flight conditions in the vertical flight, the wind direction is similar to a headwind with some sideslip, as shown in Fig. 9(a). This headwind produces additional lift assisting in a much earlier lift-off from the ground under disturbed flight conditions than that under undisturbed flight conditions. This can be observed from the Trans Flag shown in Fig. 8(a) and the altitude plot shown in Fig. 8(c).

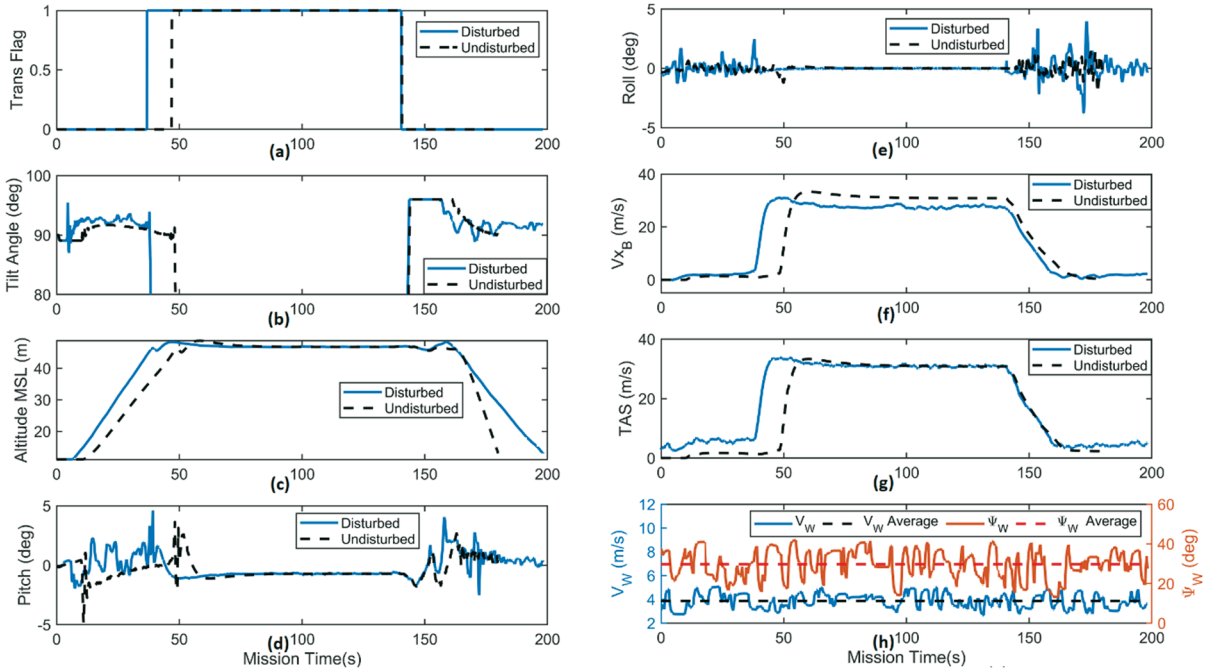

Fig. 8 Timeline plot of simulation results (a-h)

For a headwind, the thrust required to hover is slightly reduced, and so is the power requirement. Power consumption for hover flight can be minimised by aligning the nose of the aircraft against the wind (maintaining zero sideslip). This behaviour adds to the advantage of tilt-rotor over tilt-wing aircraft. However, due to the external disturbance, there is an increase in drag, and so the cruise flight under disturbed flight conditions takes more time than under undisturbed flight conditions.

Fig. 8(d) shows the pitch angle plot and the maximum deviation in pitch can be found restricted to $\pm 5^o$ even under atmospheric disturbance. Fig. 8(e) shows the roll angle plot with a deviation of about $\pm 1.5^o$ and $\pm 4^o$ in the roll during the quadcopter mode without and with atmospheric disturbance, respectively. V_{X_B} in the quadcopter mode is maintained close to zero by varying the tilt angle slightly beyond 90^o, which can be observed by comparing the tilt angle

and V_{X_B} plot in Fig. 8(b) and Fig. 8(f), respectively. The change in the true air speed (TAS) during the entire flight can also be seen in Fig. 8(g). The speed controller maintains the TAS during the cruise flight at 60 knots (30.87 m/s). The direction and velocity of the disturbance wind under disturbed flight conditions are shown in Fig. 8(h). The average wind velocity and direction were around 4 m/s and 30^o, respectively.

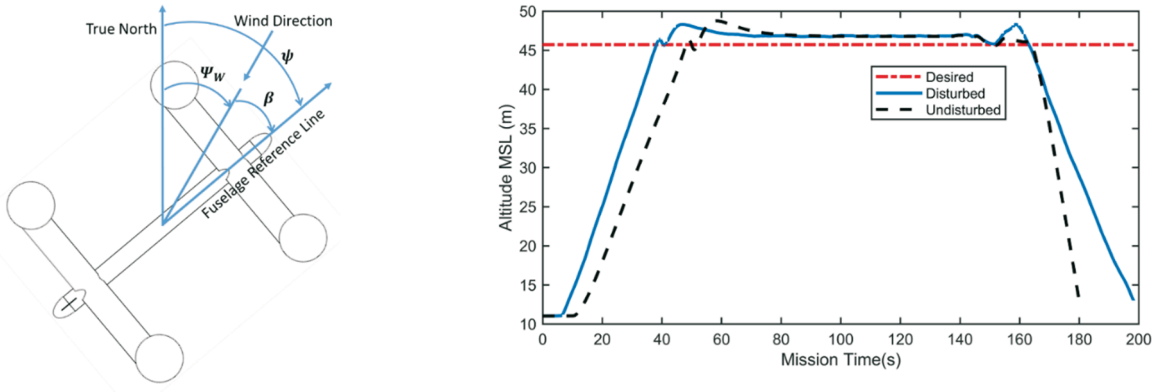

Fig. 9 (a) Disturbance wind direction definition (b) Altitude plot

Figure 9(a) shows the definition of disturbance wind direction for simulation conditions. The effect of disturbance on altitude during flight is shown in Fig. 9(b). There is a change in altitude of ± 10 ft during the transition phase, as shown in Fig. 9(b).

6.1 Transition control

Transition is one of the crucial phases of tilt rotors [3, 8, 19]. Two different controllers were implemented, one for the quadcopter mode with differential thrust control [20] and the other for the tandem mode with primary controls and a throttle. The output of the two modes is then mixed to achieve complete control. To further simplify the control, mixed signals are selectively applied based on the tilt angle and V_{X_B}. During take-off and landing only differential engine controls are provided.

During the quadcopter to the tandem mode transition ($0^o < \xi < 90^o$) the engine speeds are controlled based on the tilt angle as in equation (22). During this transition, the primary controls are fully engaged.

$$F_i(t) = [F_i(t_t)]_Q \cdot \sin\xi + [Thrust\ Command]_T \cdot \cos\xi \tag{22}$$

F_i – thrust of ith engine

$F_i(t_t)$ – thrust at the start of transition time

$[\dots]_Q$ – value corresponding to quadcopter mode

$[\dots]_T$ – values corresponding to tandem mode

During the tandem to quadcopter mode transition ($0^o < \xi < 88^o$) primary controls are fully engaged, and the throttle is made zero. During this transition period, the aircraft maintains its flight by using its kinetic energy. Differential thrust for the quadcopter mode is gradually applied once the tilt angle goes above 88^o. The thrust vector control is also fully engaged for $\xi > 88^o$.

The drop in altitude during the tandem to quadcopter mode transition due to zero throttle can be seen in Fig. 9(b). The overshoot after the drop in altitude can also be observed in the altitude plot of Fig. 9(b). The total upward force during this overshoot is the sum of hover thrust (T_H) and aerodynamic lift. From Fig. 8(g) it can be observed that during this overshoot the TAS is around 10 m/s, generating additional aerodynamic lift leading to a gain in the altitude.

Simultaneously, there is also a change in the pitch angle as the front wing generates more lift than the rear, causing a nose-up moment. The negative pitch during take-off in undisturbed flight conditions is due to the ground effect [32]. This effect is weaker in disturbed flight conditions as the aircraft lifts off at lower rotor rpm.

7. Conclusion

A tilt rotor configuration which combines the hover capability of a quadcopter and flight characteristics of a tandem wing is proposed in this paper. During the flight simulation, it is observed that an aerodynamic force is generated along the longitudinal axis as the slipstream region experiences greater airflow causing the flight to trace a slightly inclined path due to the effect of velocity component V_{X_B}. So, to address the issue of velocity component V_{X_B} thrust vector control (TVC) is implemented during take-off, hover and landing. The TVC operating angle ranges from 88^o to 110^o to cancel the generated forward force, maintaining V_{X_B}close to zero during vertical flight.

The paper also focused on presenting the practicality of the configuration based on its capability to provide smooth transition performance by designing an effective controller. The modified PID controller provides better response than the conventional PID controller in terms of reduced oscillations and actuator control effort. This high actuator control effort in the conventional PID controller becomes an issue during hardware implementation in terms of deflection limit and actuator power consumption. Tilt rotor control is achieved by mixing the signals of two separate controllers implemented for the quadcopter mode and the tandem mode. The maximum deviation in pitch is around $\pm 5^o$ and it is ± 10 ft in altitude for both disturbed and undisturbed flight conditions. The maximum deviation in roll angle is limited to $\pm 1.5^o$ and $\pm 4^o$ for simulation without and with atmospheric disturbance, respectively. The proposed scheme of transition control is found to be simple and effective in maintaining the flight with acceptable deviation in the aircraft state.

REFERENCES

[1] Kendoul, F. Survey of Advances in Guidance, Navigation, and Control of Unmanned Rotorcraft Systems, *Journal of Field Robotics* **2012**, *29* (2), 315–378. https://doi.org/10.1002/rob.20414

[2] Dimitar, D; Iliya, Z; Nikolay, M. Error and Methods for its Elimination in Systems for Measuring Parameters of Moving Objects, *Transactions of FAMENA* **2022**, *45 (4)*, 55–70, https://doi.org/ 10.21278/TOF.454029721

[3] Chenggang, L; Wenyan, Z; Jing,C; Jingjing, Y. A Comparative Study on Two Methods of Decoupling a Six-Axis Accelerometer without and with a Gyroscope, *Transactions of FAMENA* **2022**, *45 (4),* 71–83. https://doi.org/ 10.21278/TOF.454003219

[4] Liu, Z.; He, Y.; Yang, L.; Han, J. Control Techniques of Tilt Rotor Unmanned Aerial Vehicle Systems: A Review, *Chinese Journal of Aeronautics* **2017**, *30* (1), 135–148. https://doi.org/10.1016/j.cja.2016.11.001

[5] Saeed, A. S.; Younes, A. B.; Cai, C.; Cai, G. A Survey of Hybrid Unmanned Aerial Vehicles, *Progress in Aerospace Sciences* **2018**, *98* (March), 91–105. https://doi.org/10.1016/j.paerosci.2018.03.007

[6] Taha öner, K.; Çetinsoy, E.; Sirimoğlu, E.; Hançer, C.; Ünel, M.; Akşit, M. F.; Gülez, K.; Kandemir, I. Mathematical Modeling and Vertical Flight Control of a Tilt-Wing UAV, *Turkish Journal of Electrical Engineering and Computer Sciences* **2012**, *20* (1), 149–157. https://doi.org/10.3906/elk-1007-624

[7] Abhishek, A.; Krishna, M. R.; Sinha, S.; Bhowmik, J.; Das, D. Design, Development and Flight Testing of a Novel Quadrotor Convertiplane Unmanned Air Vehicle, *Annual Forum Proceedings - AHS International* **2017**, 205–218.

[8] Hochstenbach, M.; Notteboom, C.; Theys, B.; De Schutter, J. Design and Control of an Unmanned Aerial Vehicle for Autonomous Parcel Delivery with Transition from Vertical Take-off to Forward Flight - VertiKUL, a Quadcopter Tailsitter, *International Journal of Micro Air Vehicles* **2015**, *7* (4), 395–405. https://doi.org/10.1260/1756-8293.7.4.395

[9] Raj, N.; Banavar, R.; Abhishek; Kothari, M. Attitude Control of Novel Tail Sitter: Swiveling Biplane–Quadrotor, *Journal of Guidance, Control, and Dynamics* **2020**, *43* (3), 599–607. https://doi.org/10.2514/1.G004697

[10] Yuksek, B.; Vuruskan, A.; Ozdemir, U.; Yukselen, M. A.; Inalhan, G. Transition Flight Modeling of a Fixed-Wing VTOL UAV, *Journal of Intelligent & Robotic Systems* **2016**, *84* (1–4), 83–105. https://doi.org/10.1007/s10846-015-0325-9

[11] Quantum tron. http://www. quantum-systems.com/products/quantum-tron. Accessed 5 Jul 2021

[12] Hrvoje, B; Josip, K. Chattering-Free Tracking Control of a Fully Actuated Multirotor with Passively Tilted Rotors, *Transactions of FAMENA* **2018**, *42 (1),* 1–14, https://doi.org/ 10.21278/TOF.42101

[13] Lambert, T.; Warbecq, N.; Hendrick, P.; Nudds, R.; Andrianne, T.; Dimitriadis, G. Numerical and Experimental Investigation of Tandem Wing Flyers,. *AIAA Scitech 2019 Forum* **2019**, No. January. https://doi.org/10.2514/6.2019-1620

[14] Craighead, J.; Murphy, R.; Burke, J.; Goldiez, B. A Survey of Commercial & Open Source Unmanned Vehicle Simulators, *Proceedings - IEEE International Conference on Robotics and Automation* **2007**, No. April, 852–857. https://doi.org/10.1109/ROBOT.2007.363092

[15] Agha, M.; Kanistras, K.; Saka, P. C.; Valavanis, K.; Rutherford, M. System Identification of Circulation Control UAV Using X-Plane Flight Simulation Software and Flight Data, In *AIAA Modeling and Simulation Technologies Conference*; American Institute of Aeronautics and Astronautics: Reston, Virginia, 2017. https://doi.org/10.2514/6.2017-3154

[16] Lai, Y. C.; Le Tri, Q. System Identification and Control of a Small Unmanned Helicopter at Hover Mode, In *2017 2nd International Conference on Control and Robotics Engineering, ICCRE 2017*; IEEE, 2017; pp 92–96. https://doi.org/10.1109/ICCRE.2017.7935049

[17] Agha, M.; Kanistras, K.; Rutherford, M. J.; Valavanis, K. P. Mathematical Model Derivation of an Unmanned Circulation Control Aerial Vehicle UC2AV, *Control Theory and Technology* **2020**, *18* (1), 1–18. https://doi.org/10.1007/s11768-020-8151-4

[18] Prabhu, S; Anitha, G. An innovative analytic redundancy approach to air data sensor fault detection, *The Aeronautical Journal* **2020**, *124 (1273),* 346–367. https://doi.org/ 10.1017/aer.2019.143

[19] Junior, J. M. M.; Khamvilai, T.; Sutter, L.; Feron, E. Test Platform for Autopilot System Embedded in a Model of Multi-Core Architecture Using X-Plane Flight Simulator, In *2019 IEEE/AIAA 38th Digital Avionics Systems Conference (DASC)*; IEEE, 2019; Vol. 2019-Septe, pp 1–6. https://doi.org/10.1109/DASC43569.2019.9081788

[20] Silva, N. B. F.; Fontes, J. V. C.; Branco, K. R. L. J. C. Control Validation with Software-in-the-Loop for a Fixed-Wing Vertical Takeoff and Landing Unmanned Aerial Vehicle with Multiple Flight Stages, In *Proceedings - International Symposium on Computers and Communications*; 2019; Vol. 2019-June, pp 1222–1227. https://doi.org/10.1109/ISCC47284.2019.8969571

[21] Guang, H; Li, Y; Shengde, J; Xiangke, W. Simulation verification of Flight Control of a tilt tri-rotor UAV Using X-plane, In *39th Chinese Control Conference, IEEE,* 2020, pp 7008–7013. https://doi.org/ 10.23919/CCC50068.2020.9188535

[22] Senthil, K. S; Anitha, G. A Novel Self-Tuning Fuzzy Logic-Based PID Controllers for TwoAxis Gimbal Stabilization in a Missile Seeker, *International Journal of Aerospace Engineering*, **2021**, 2021. https://doi.org/ 10.1155/2021/8897556

[23] Yechout, T. R.; Morris, S. L.; Bossert, D. E.; Hallgren, W. F. *Introduction to Aircraft Flight Mechanics: Performance, Static Stability, Dynamic Stability, and Classical Feedback Control*; AIAA: USA, 2003.

[24] Hadytama, M. R.; Sasongko, R. A. Modelling and Control of Tilt-Rotor Longitudinal Dynamics in Transition Phase, In *2017 5th International Conference on Instrumentation, Communications, Information Technology, and Biomedical Engineering (ICICI-BME)*; IEEE, 2017; pp 39–44. https://doi.org/10.1109/ICICI-BME.2017.8537741

[25] Mahony, R.; Kumar, V.; Corke, P. Multirotor Aerial Vehicles: Modeling, Estimation, and Control of Quadrotor, *IEEE Robotics & Automation Magazine* **2012**, *19*(3), 20–32. https://doi.org/10.1109/MRA.2012.2206474

[26] X-Plane 10 Desktop Manual https://www.x-plane.com/files/manuals/X-Plane_10_Desktop_manual.pdf (accessed 2021 -06 -28).

[27] Plane Maker Manual for X-Plane 10 https://www.x-plane.com/files/manuals/Plane_Maker_manual.pdf (accessed 2021-06-28).

[28] Stojcsics, D. Autonomous Waypoint-Based Guidance Methods for Small Size Unmanned Aerial Vehicles, *Acta Polytechnica Hungarica* **2014**, *11* (10), 215–233. https://doi.org/10.12700/APH.11.10.2014.10.13

[29] Rengarajan, M; Anitha, G. Algorithm Development and Testing of Lowcost Waypoint Navigation System, *IRACST -Engineering science and technology: An International Journal* **2013**, *3 (2),* 411–415.

[30] Hong, J. W.; Ansell, P. J. Influence of Freestream Velocity on Tilt-Rotor Fountain Effect, *Journal of Aircraft* **2018**, *55* (4), 1742–1745. https://doi.org/10.2514/1.C034599

[31] Cetinsoy, E.; Dikyar, S.; Hancer, C.; Oner, K. T.; Sirimoglu, E.; Unel, M.; Aksit, M. F. Design and Construction of a Novel Quad Tilt-Wing UAV, *Mechatronics* **2012**, *22* (6), 723–745. https://doi.org/10.1016/j.mechatronics.2012.03.003

[32] Radhakrishnan, A.; Schmitz, F. Quad Tilt Rotor Aerodynamics in Ground Effect, In *23rd AIAA Applied Aerodynamics Conference*; American Institute of Aeronautics and Astronautics: Reston, Virigina, 2005; Vol. 2, pp 1290–1300. https://doi.org/10.2514/6.2005-5218

Submitted: 11.8.2021

Accepted: 04.01.2023

Saravanan Elanchezhian*, Teaching Fellow
Anitha G, Associate Prof.,
Department of Aerospace Engineering,
MIT Campus, Anna University, Chennai, India
*Corresponding author:
saravanan.elanchezhian@yahoo.com